Disturbance Observer Based PBC for Static Synchronous Compensator under System Disturbances

Jinmu Lai, *Student Member, IEEE*, Xin Yin, *Member, IEEE*, Lin Jiang, *Member, IEEE*, Xianggen Yin, *Member, IEEE*, Zhen Wang and Zia Ullah

***Abstract*- Passivity-based control (PBC) relies on an accurate mathematical model and thus its performance will be degraded by the weak robustness against to parameters uncertainties, modeling error, and external disturbances. Moreover, it cannot achieve zero tracking error of the steady-state current under parameters uncertainties and modeling error. This paper proposes a novel disturbance observer (DO) based PBC (DO-PBC) for static synchronous compensator (STATCOM) to achieve better stability and dynamic performances against disturbances. A DO that has been introduced into the PBC current loop is used to compensate system disturbances, which can improve the robustness of the control system and eliminate the steady-state tracking error. Moreover, the proposed DO-PBC provides faster responses in handling various kinds of disturbances. Then, the detail design process, stability and robustness analysis, and parameters tuning method are investigated and presented. Also, the proposed method is simple to be implemented by the separation principal. The performance comparisons among the PI, the conventional PBC, and the proposed DO-PBC are carried out to show the effectiveness of the proposed method against disturbances and the precise current tracking, via simulation tests and experimental tests based on a down-scale laboratory prototype experiment of 380 V STATCOM.[1]**

***Index Terms*- Static synchronous compensator, passivity-based control, disturbance observer, system disturbances.**

I. Introduction

In recent years, reactive power fluctuations in distribution networks are more frequent due to the penetration of plug-and-play renewable energy resources, electric vehicle charging piles and distributed storage devices [1]. Static synchronous compensator (STATCOM) plays a vital role in energy saving and power quality control of modern distribution networks. STATCOM, with fully-controlled power electronic devices, becomes more and more attractive in distribution networks due to their fast response, efficient performance and small size [2, 3]. The cascaded H-bridge (CHB) STATCOM is one of the well-known multilevel STATCOM topologies [4, 5], which provides the required multilevel output voltage based on the series connection of H-bridge cells.

The main task of the STATCOM's controller is to achieve fast, stable and accurate tracking of the reference value during operation. Also, the controller is required to have strong robustness which that can handle frequent changes in operating conditions and disturbances of the system. Various current control approaches have been proposed in the literature [6-15]. Proportional-integral (PI) -based controllers are the most widely used and easy-to-tuned ones based on rotating reference frame [6, 7], their performance is degraded by the frequently changed operation points and the system disturbances consisting of parameters uncertainties, modeling errors and disturbances. PI-type controllers is not easy to guarantee the uniform and satisfactory control performance over different operating conditions [8]. In [9], an adaptive PI control scheme has been adopted to realize the desired response of STATCOM for voltage regulation during a disturbance. However, the adaptive PI depends highly on the design of identification laws on time-varying operation condition or parameters. In [10], multivariable-PI current control was proposed for voltage source converters to provide fast dynamic and a zero steady-state error. Although the multivariable-PI controller achieves well performance, however, the *d*- and *q*- axes cannot be fully decoupled since this method relies on precisely model of the plant. Based on this, a robust optimization-based multivariable-PI current controller (OMCC) [11, 12] was proposed to obtain better dynamic performance and superior decoupling capability. In [13], the finite control set model predicts control (FCS-MPC) for CHB STATCOM was presented to achieve high dynamic performance. However, the main drawback of FCS-MPC is that the quality of the MPC algorithm depends on the modeling accuracy of the system, raising concerns about robustness against parametric uncertainties. Sliding mode control [14] has been introducing to design a simple and robust controller for STATCOM. Although this method has good abilities against parameter perturbations and disturbances, it suffers from chattering problem. Recently, Passivity-based Control (PBC) has received significant

This work was supported by the Funds for National Natural Science Foundation of China (No. 51877089, No. 51277084) and National Key Research and Development Program of China (No. 2017YFB0902900).

Jinmu Lai, Xianggen Yin, Zhen Wang and Zia Ullah are with State Key Laboratory of Advanced Electromagnetic Engineering and Technology, Huazhong University of Science and Technology, Wuhan, 430074, P. R. China. (E-mail: laijinmu@hust.edu.cn; xgyin@hust.edu.cn; wangzhen2016@hust.edu.cn; ziaullah@hust.edu.cn).

Xin Yin (*Corresponding author*) and Lin Jiang are with Department of Electrical Engineering and Electronics, The University of Liverpool, Liverpool, UK (E-mail: xin.yin@liverpool.ac.uk; ljiang@liverpool.ac.uk).

attention in the power converters control [15-32]. The PBC method is an energy-shaping-based approach which considers the system energy dissipation and with merits of high dynamic performance, clear physical meaning, as well as, its simplicity tuning process, makes it a powerful control strategy in power electronics [15]. The application of PBC on power electronics can be found in high voltage direct current (HVDC) system [16], DC/DC converter [17], doubly-fed induction machine [18], the integration of distributed generation [19], solid-state transformer [20], and three-phase front-end power converter [21-23].

A PBC approach has been already applied to STATCOM system. As introduced in [5, 24], the current loop of the converter was well controlled by PBC method. In [25], PBC for a type 2 STATCOM with nonlinear damping was designed to improve the control performance. However, it should be pointed out that PBC approach [18-25] is kind of model-based control where parameters uncertainties may result in a steady-state error [26]. Recently researches are trying to eliminate steady-state error caused by the conventional PBC under parameters uncertainties. In order to handle the steady-state current error of the conventional PBC, a PI regulator is inserted into the coupling terms of the modified PBC in [26] for shunt STATCOM. PBC combined with an auxiliary sliding mode control strategy was proposed to increase the system robustness and thereby reduce the steady-state tracking error [27]. Lyapunov stability theory based parameter estimation law was designed for adaptive PBCs to deal with robustness issue of parameter uncertainties [28, 29]. However, these adaptive PBC approaches are hard to estimate the time-varying unknown parameters and the time-varying external disturbance. In [30], a perturbation observer-based robust passivity-based control scheme was proposed for multi-terminal VSC-HVDC system, via a high-gain state and perturbation observer to estimate disturbance. A generalized proportional integral (GPI) observer-based active disturbance rejection (ADR) PBC method is designed for buck-boost DC-DC converter [31, 32]. However, those time-domain observers require many controller parameters need to be tuned, and the robust stability and performance for the designed strategy should be investigated further.

This paper investigates a robust PBC for STATCOM to encounter the effects of various disturbances which include parameters uncertainties, modeling errors and external disturbances. The system disturbances are estimated by DO proposed in [33-36] and applied to attenuate the impact of the real disturbances. The DO-PBC does not require an accurate STATCOM model and the tuning process is simple to implement. The global stability and the robustness of DO-PBC method under system disturbances conditions have been investigated analytically. Compared with the PI and the conventional PBC, the proposed DO-PBC can achieve zero steady-state current tracking error under parameters uncertainties, with a quicker dynamic response, better decoupling between the *d*- and *q*- channels, and faster responses in handling not only constant disturbances but also many other types of disturbances, including the parameter uncertainties, unmodeled dynamic, and external disturbances. Simulation and experimental tests are carried out to verify the effectiveness.

This paper is organized as follows. Section II investigates the robustness performance of the conventional PBC method. A composite DO-PBC method is proposed in Section III. In Section IV, a hierarchical DC-link voltage control is employed to balance voltage and generate the reference currents for positive- and negative-sequences DO-PBC. In Section V, simulation results are presented to verify the proposed method. The experimental results are given in Section VI. Section VII gives the conclusion.

II. Conventional PBC Method

Fig. 1 shows the schematic structure of the transformerless star-configured CHB STATCOM system. L and R are the actual inductance and resistance of the L-filter. u_{sa}, u_{sb} and u_{sc} are the voltages of the point of common coupling. u_a, u_b and u_c are the voltages of the STATCOM side. i_{sa}, i_{sb} and i_{sc} are the three-phase current of the grid. i_a, i_b and i_c are the three-phase current of STATCOM. i_{la}, i_{lb} and i_{lc} are the three-phase current of the load.

The main task of the STATCOM's controller is to achieve fast, stable and accurate tracking of the reference value during operation. In this section, we will investigate how the conventional PBC depends much on the model parameters of the plant. Robustness analysis of conventional PBC will be discussed in detail.

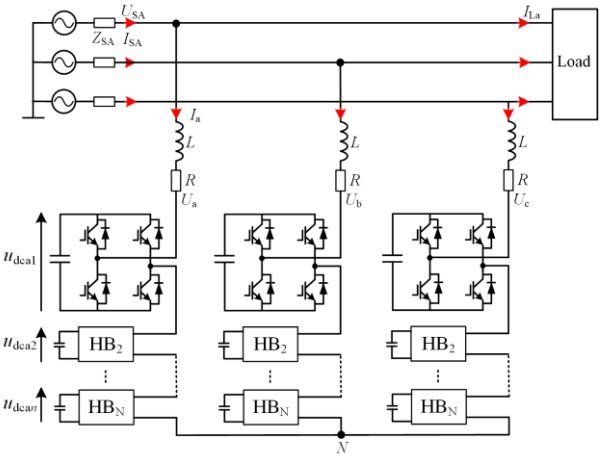

Fig. 1 Topology of transformerless N-cell CHB STATCOM.

A. Conventional PBC

Referring to Fig.1, the voltage and current equations in the *d-q* frame can be obtained as

$$\begin{cases} L_n \dfrac{di_d}{dt} = u_{sd} + \omega L_n i_q - i_d R_n - u_d \\ L_n \dfrac{di_q}{dt} = u_{sq} - \omega L_n i_d - i_q R_n - u_q \end{cases} \tag{1}$$

where L_n and R_n are the nominal inductance and the equivalent resistance of L-filter, respectively. i_d, i_q, u_d, u_q, u_{sd}, u_{sq} are the *d*-axis and *q*-axis components corresponding to the three-phase injection current, STATCOM cluster voltage, and grid

voltage, respectively. ω=314 rad/s is the angular synchronous frequency.

For convenience (1) can be rewritten in the form of the Euler Lagrange equation as

$$\boldsymbol{M}\dot{\boldsymbol{x}} \quad \boldsymbol{J}\boldsymbol{x} \quad \boldsymbol{R}\boldsymbol{x} = \boldsymbol{F} \tag{2}$$

$$\boldsymbol{M} = \begin{bmatrix} L_\mathrm{n} & 0 \\ 0 & L_\mathrm{n} \end{bmatrix}, \quad \boldsymbol{J} = \begin{bmatrix} 0 & -\omega L_\mathrm{n} \\ \omega L_\mathrm{n} & 0 \end{bmatrix} \boldsymbol{R} = \begin{bmatrix} R_\mathrm{n} & 0 \\ 0 & R_\mathrm{n} \end{bmatrix},$$

$$\boldsymbol{F} = \begin{bmatrix} u_\mathrm{sd} - u_\mathrm{d} \\ u_\mathrm{sq} - u_\mathrm{q} \end{bmatrix}, \boldsymbol{x} = \begin{bmatrix} i_\mathrm{d} \\ i_\mathrm{q} \end{bmatrix}$$

where $\boldsymbol{x}$ is the state variables. $\boldsymbol{M}$ is the positive definite matrix. $\boldsymbol{J}$ is the anti-symmetric matrix. $\boldsymbol{R}$ is the positive definite matrix, describing the dissipation characteristic of the system. $\boldsymbol{F}$ is the external input matrix which reflects the energy exchange between the STATCOM and the power grid.

If the reference output current of STATCOM is defined as $\boldsymbol{x}^*=[i_\mathrm{d}^* \; i_\mathrm{q}^*]^\mathrm{T}$, the tracking error current can be written as

$$\boldsymbol{x}_\mathrm{e} = \boldsymbol{x} - \boldsymbol{x}^* = \begin{bmatrix} i_\mathrm{d} - i_\mathrm{d}^* \\ i_\mathrm{q} - i_\mathrm{q}^* \end{bmatrix} \tag{3}$$

In order to improve the dynamic tracking performance of the control system, an additional dissipative damping $\boldsymbol{R}_\mathrm{d}$ is added via feedback control to accelerate the error energy dissipation. One can be obtained with additional damping $\boldsymbol{R}_\mathrm{d}$ by substituting (3) into (2).

$$\boldsymbol{M}\dot{\boldsymbol{x}} \quad \boldsymbol{J}\boldsymbol{x} \quad \boldsymbol{R}\,\boldsymbol{x} \quad \boldsymbol{F} \quad \boldsymbol{M}\dot{\boldsymbol{x}} \quad \boldsymbol{J}\boldsymbol{x} \quad \boldsymbol{R}\boldsymbol{x} \quad \boldsymbol{R}\,\boldsymbol{x}_\mathrm{e}) = \boldsymbol{\Delta} \tag{4}$$

where $\boldsymbol{R}_\mathrm{a}=\boldsymbol{R}+\boldsymbol{R}_\mathrm{d}$, $\boldsymbol{R}_\mathrm{d}$=diag($r_\mathrm{d}$, r_d), and r_d>0.

In order to analyze the global asymptotic stability and evaluate the rate of asymptotic convergence, error energy (Lyapunov) function is defined as

$$E = 0.5L_\mathrm{n}((i_\mathrm{d} - i_\mathrm{d}^*)^2 + (i_\mathrm{q} - i_\mathrm{q}^*)^2) = 0.5\boldsymbol{x}_\mathrm{e}^\mathrm{T}\mathbf{M}\boldsymbol{x}_\mathrm{e} \tag{5}$$

It can be observed from (5) that a good enough reference current can obtain smaller error energy, and the convergence rate can be evaluated by the change rate of the error energy, i.e. $\dot{E}$. According to the Lyapunov stability theorem, if there exists

$$\dot{E} \qquad {}_{\mathrm{BC}} < 0, \;\; \tau_\mathrm{PBC} > 0 \tag{6}$$

Then, the system converges exponentially to the expected equilibrium point, and its convergence rate is determined by τ_PBC. Taking the time derivative of (5) then yields

$$\dot{E} \quad \boldsymbol{x} \quad \boldsymbol{M}\dot{\boldsymbol{x}} \qquad {}_\mathrm{n} + r_\mathrm{d})/L_\mathrm{n})E = -E/\tau_\mathrm{PBC} < 0 \tag{7}$$

where τ_PBC=0.5L_n/(R_n+r_d) represents the time constant of control system.

Since E>0 and $\dot{E}$ <0 according to (5) and (7), based on the Lyapunov stability theorem, the current loop control is asymptotically stable. The smaller theτ_PBC, the faster the convergence speed. Therefore, a suitable injection dissipative damping r_d can be selected to achieve an efficient dynamic response.

Through the above analysis and considering dq-axis current decoupling, the PBC control law can be obtained as

$$\boldsymbol{F} - (\boldsymbol{M}\dot{\boldsymbol{x}} \quad \boldsymbol{J}\,\boldsymbol{x} \; + \boldsymbol{x}_\mathrm{e}) + \boldsymbol{R}\boldsymbol{x}^* - \boldsymbol{R}_\mathrm{d}\boldsymbol{x}_\mathrm{e}) = 0 \tag{8}$$

The control law can be explicitly rewritten as

$$\begin{cases} u_\mathrm{d} = -L_\mathrm{n}\dfrac{\mathrm{d}i_\mathrm{d}^*}{\mathrm{d}t} + \omega L_\mathrm{n} i_\mathrm{q} - R_\mathrm{n} i_\mathrm{d}^* + r_\mathrm{d}(i_\mathrm{d} - i_\mathrm{d}^*) + u_\mathrm{sd} \\ u_\mathrm{q} = -L_\mathrm{n}\dfrac{\mathrm{d}i_\mathrm{q}^*}{\mathrm{d}t} - \omega L_\mathrm{n} i_\mathrm{d} - R_\mathrm{n} i_\mathrm{q}^* + r_\mathrm{d}(i_\mathrm{q} - i_\mathrm{q}^*) + u_\mathrm{sq} \end{cases} \tag{9}$$

B. Robustness Analysis

According to (1) and (9), the PBC scheme can be expressed using the transform function block in s-domain, as shown in Fig. 2. $P(s)$=1/(sL+R) is the actual plant. $P_\mathrm{n}(s)$=1/(sL_n+R_n) is the nominal plant. $d(s)$ is the disturbance.

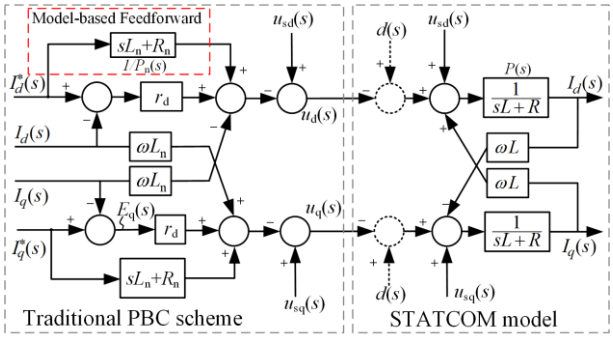

Fig. 2 Block diagram of the passivity-based control.

It can be observed that the conventional PBC scheme is, in essence, a compound control, which contains feedback term and model-based inverse feedforward term. The feedback term is similar to the conventional P control, while the model-based inverse input is used as feedforward to improve the output tracking performance.

The closed-loop transfer function of the conventional PBC-based STATCOM shown in Fig.2 can be derived as

$$\begin{bmatrix} I_\mathrm{d}(s) \\ I_\mathrm{q}(s) \end{bmatrix} = \begin{bmatrix} G_\mathrm{dd} & G_\mathrm{dq} \\ G_\mathrm{qd} & G_\mathrm{qq} \end{bmatrix} \begin{bmatrix} I_\mathrm{d}^*(s) \\ I_\mathrm{q}^*(s) \end{bmatrix} \tag{10}$$

where

$$\begin{cases} G_\mathrm{dd} = \dfrac{I_\mathrm{d}(s)}{I_\mathrm{d}^*(s)} = G_\mathrm{qq} = \dfrac{I_\mathrm{q}(s)}{I_\mathrm{q}^*(s)} = \dfrac{(sL_\mathrm{n} + R_\mathrm{n} + r_\mathrm{d})(sL + R + r_\mathrm{d})}{(sL + R + r_\mathrm{d})^2 + (\omega L - \omega L_\mathrm{n})^2} \\ G_\mathrm{dq} = \dfrac{I_\mathrm{d}(s)}{I_\mathrm{q}^*(s)} = -G_\mathrm{qd} = \dfrac{I_\mathrm{q}(s)}{I_\mathrm{d}^*(s)} = \dfrac{(sL_\mathrm{n} + R_\mathrm{n} + r_\mathrm{d})(\omega L - \omega L_\mathrm{n})}{(sL + R + r_\mathrm{d})^2 + (\omega L - \omega L_\mathrm{n})^2} \end{cases} \tag{11}$$

The error transfer function $I_\mathrm{q}^*(s)$ to $E_\mathrm{q}(s)$ is given by

$$G_\mathrm{E} = \frac{E_\mathrm{q}(s)}{I_\mathrm{q}^*(s)} = \frac{(sL + R - sL_\mathrm{n} - R_\mathrm{n})(sL + R + r_\mathrm{d}) + (\omega L - \omega L_\mathrm{n})^2}{(sL + R + r_\mathrm{d})^2 + (\omega L - \omega L_\mathrm{n})^2} \tag{12}$$

For the conventional PBC, it can be found that, if and only if $P(s)$=$P_\mathrm{n}(s)$, the output current can track the reference current with zero steadystate error, i.e. G_E=0, and the coupling terms between d-axis and q-axis (G_dq=G_qd=0) can be eliminated clearly. With the model-based inverse feedforward input, i.e. $I_\mathrm{q}^*/P_\mathrm{n}(s)$, we obtain exact-output tracking with ideal response characteristics. It is noted that the model-based inverse

feedforward input realizes exact tracking the reference input without system disturbances. Moreover, feedback (in conjunction with the inverse input) must still be used to accelerate the error energy dissipation and correct for tracking error.

However, in fact, unavoidable disturbances, including parameters uncertainties, modeling error and external disturbances, may occur for STATCOM.

When external disturbance $d(s)$ exists, the close-loop transfer function from disturbance $d(s)$ to the output $I_q(s)$ is

$$G_{dI_q} = \frac{I_q(s)}{d(s)} = \frac{(sL+R+r_d)-(\omega L-\omega L_n)}{(sL+R+r_d)^2+(\omega L-\omega L_n)^2} \quad (13)$$

It can be seen that the external disturbance will produce a transient component to the output current. The transient disturbance component may affect the quality of the compensation current.

On the other hand, the actual plant $P(s)$ may not be known exactly due to temperature, core saturation, and other environmental conditions, that means the zero steady state error compensation condition ($P(s)=P_n(s)$) is almost impossible to satisfy. The parameters can be formalized as $L=L_n+\Delta L$ and $R=R_n+\Delta R$. ΔL and ΔR are the parameters deviation. Obviously, in the conventional PBC method, although the output current can quickly converge to the steady state under the system disturbances, there is always a steady-state error, i.e. $G_E|_{t\to\infty}\neq 0$, and the exact tracking of the reference current cannot be achieved. Moreover, the coupling terms always exist, i.e. $G_{qd}\neq 0$ and $G_{dq}\neq 0$, which will affect the dynamic performance.

III. Proposed Disturbance-Observer-Based PBC Method

A. Disturbance-observer-based PBC

As mentioned previously, due to system disturbances, the conventional PBC method may result in a steady-state error and coupling terms. In order to improve the robustness of the controller, a novel PBC combined with plug-in observer technique is proposed in this section.

Fig. 3 shows a block diagram of DOB [34]. $P(s)$ is the actual plant, $P_n(s)$ is the nominal plant, $Q(s)$ is the lower pass filter, $U_r(s)$ is the reference signal, $U(s)$ is the controller output, $Y(s)$ is the system output, $\xi(s)$ is the measurement noise, $d(s)$ is the disturbance, and $\tilde{d}(s)$ is the estimate of the system disturbances (including parameters uncertainties, modeling error and external disturbances).

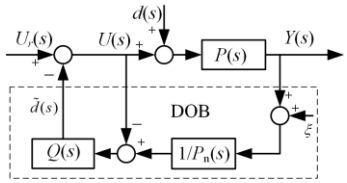

Fig. 3 Block diagram of DOB.

Based on the block diagram in Fig. 3, the estimate of the system disturbances is

$$\tilde{d}(s) = [(P(s)-P_n(s))U(s)+P(s)d(s)+\xi(s)]Q(s)/P_n(s) \quad (14)$$

And the system output Y(s) can be written as

$$Y(s) = G_{U_rY}(s)U_r(s)+G_{dY}(s)d(s)+G_{\xi Y}(s)\xi(s) \quad (15)$$

where

$$G_{U_rY}(s) = \frac{P(s)P_n(s)}{P_n(s)+(P(s)-P_n(s))Q(s)} \quad (16)$$

$$G_{dY}(s) = \frac{P(s)P_n(s)(1-Q(s))}{P_n(s)+(P(s)-P_n(s))Q(s)} \quad (17)$$

$$G_{\xi Y}(s) = \frac{-P(s)Q(s)}{P_n(s)+(P(s)-P_n(s))Q(s)} \quad (18)$$

Notice that $1/P_n(s)$ may be anti-causal. Therefore, the relative degree of the filter $Q(s)$ should be higher than that of $1/P_n(s)$ to ensure that $Q(s)/P_n(s)$ is realizable.

Since the disturbances $d(s)$ are dominant in the low frequency, while the noise $\xi(s)$ is dominant in the high frequency range, within the bandwidth of $Q(s)$, i.e., $Q(s)=1$, the system output $Y(s)$ (15) can be rewritten as

$$Y(s) = P_n(s)U_r(s) \quad (19)$$

Based on (19), a conclusion can be made that the actual plant $P(s)$ is forced to behave as the nominal plant $P_n(s)$ without the system disturbances. That is to say, the external disturbance and parameters uncertainties can be completely eliminated.

In order to achieve zero steady-state current tracking error and realize the decoupling, a DO-PBC scheme is proposed in this paper. Fig. 4 shows the framework of the proposed DO-PBC scheme. The meanings of each term are the same as those in Fig.2 and Fig.3. The controller design and robustness analysis of the proposed DO-PBC are presented as follows.

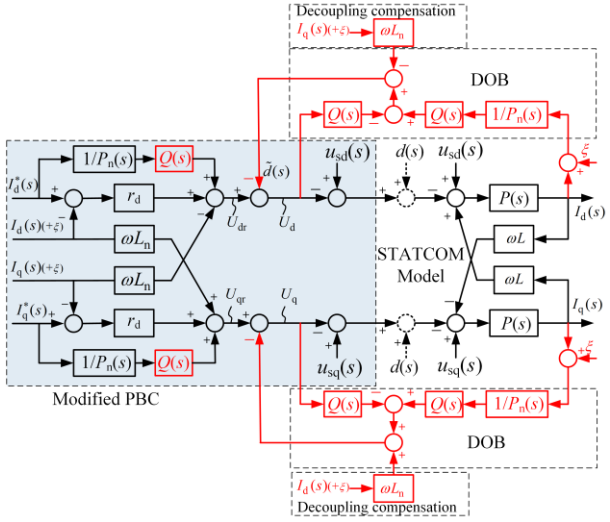

Fig. 4 Block diagram of the proposed DO-PBC.

Based on the equivalent transfer function block diagram as shown in Fig. 4 and without considering disturbances $d(s)$ and measurement noise ξ, the closed-loop transfer function of the proposed DO-PBC with STATCOM can be derived as

$$\begin{bmatrix} I_{\mathrm{d}}(s) \\ I_{\mathrm{q}}(s) \end{bmatrix} = \begin{bmatrix} G'_{\mathrm{dd}} & G'_{\mathrm{dq}} \\ G'_{\mathrm{qd}} & G'_{\mathrm{qq}} \end{bmatrix} \begin{bmatrix} I^*_{\mathrm{d}}(s) \\ I^*_{\mathrm{q}}(s) \end{bmatrix} \tag{20}$$

where

$$\begin{cases} G'_{\mathrm{dd}} = \dfrac{I_{\mathrm{d}}(s)}{I^*_{\mathrm{d}}(s)} = G'_{\mathrm{qq}} = \dfrac{I_{\mathrm{q}}(s)}{I^*_{\mathrm{q}}(s)} = \dfrac{P(Q + r_{\mathrm{d}}P_{\mathrm{n}})M}{M^2 + N^2} \\ G'_{\mathrm{dq}} = \dfrac{I_{\mathrm{d}}(s)}{I^*_{\mathrm{q}}(s)} = -G'_{\mathrm{qd}} = \dfrac{I_{\mathrm{q}}(s)}{I^*_{\mathrm{d}}(s)} = \dfrac{P(Q + r_{\mathrm{d}}P_{\mathrm{n}})N}{M^2 + N^2} \\ M = r_{\mathrm{d}}P_{\mathrm{n}}P + PQ + (1-Q)P_{\mathrm{n}}, \quad N = (1-Q)\omega L P_{\mathrm{n}} P \end{cases} \tag{21}$$

Analogously, the error transfer function $I^*_{\mathrm{q}}(s)$ to $E_{\mathrm{q}}(s)$ is given by

$$G'_{\mathrm{E}} = \frac{E_{\mathrm{q}}(s)}{I^*_{\mathrm{q}}(s)} = \frac{M^2 + N^2 - P(Q + r_{\mathrm{d}}P_{\mathrm{n}})M}{M^2 + N^2} \tag{22}$$

Within the bandwidth of $Q(s)$, i.e., $Q(s)$=1, the closed-loop transfer functions G'_{dd}, G'_{qq} and coupling transfer function G'_{dq}, G'_{qd} can be expressed as (23) that indicates, G'_{dd} and G'_{qq} will be equal to 1. It implies that, whether the system disturbances occur or not, the *d*-axis and *q*-axis current loop can track the current references at the bandwidth of $Q(s)$ with zero steady-state error under the proposed method. Moreover, the coupling branch transfer function G'_{dq}, G'_{qd} always equal to 0. The coupling path is eliminated completely.

$$\begin{cases} G'_{\mathrm{dd}} = G'_{\mathrm{qq}} = \dfrac{(r_{\mathrm{d}}P_{\mathrm{n}}P + P)}{(r_{\mathrm{d}}P_{\mathrm{n}}P + P)} = 1 \\ G'_{\mathrm{dq}} = G'_{\mathrm{qd}} = 0 \end{cases} \tag{23}$$

The closed-loop transfer function from disturbance $d(s)$ and measurement noise ξ to the output $I_{\mathrm{q}}(s)$ can be derived as

$$\begin{cases} G'_{\xi\mathrm{q}} = \dfrac{I_{\mathrm{q}}(s)}{\xi(s)} = \dfrac{P(Q + r_{\mathrm{d}}P_{\mathrm{n}})(N - M)}{M^2 + N^2} \\ G'_{\mathrm{dis}} = \dfrac{I_{\mathrm{q}}(s)}{d(s)} = \dfrac{P_{\mathrm{n}}P(1-Q)(M - N)}{M^2 + N^2} \end{cases} \tag{24}$$

Within the bandwidth of $Q(s)$, the external disturbance $d(s)$ will be attenuated according to (24).

It can be observed from (23) and (24) that the DO-PBC method can reject inaccurate parameters, disturbances and filter out noise within the bandwidth of $Q(s)$. However, it can be seen from (21) that improper design of $Q(s)$ will lead to the denominator of (21) is not Hurwitz. Therefore, it is worth to give the efficient design method of a $Q(s)$ to assure the robustness of the proposed method. We assume the $Q(s)$ of the following form:

$$Q(s) = \frac{\sum_{i=0}^{n} a_{mi}(\tau s)^i}{(\tau s + 1)^m} \tag{25}$$

where τ is the filter time constant, a_{mi}=m!/(m-1)!i! is the binomial coefficient, m is the denominator order and n is the numerator order. Since the plant can be described by the first order transfer function $P(s)$=1/(sL+R), the condition (m-n≥1) should be satisfied so that the transfer function $Q(s)/P_{\mathrm{n}}(s)$ becomes proper. Moreover, (18) suggests that a high bandwidth $Q(s)$ will increase the system sensitivity to measurement noise. It is preferred to use the smaller m and n that makes the controller proper to avoid complexity. In this paper, m=3, n=1 are chosen [36]. Then, $Q(s)$ can be rewritten as

$$Q(s) = \frac{3\tau s + 1}{(\tau s)^3 + 3(\tau s)^2 + 3\tau s + 1} \tag{26}$$

B. Robustness Analysis

In order to highlight the benefits of proposed DO-PBC method, the pole-zero locations of the closed-loop system, step response and the closed-loop Bode plots of G'_{qq} and G'_{dq} are shown in Fig. 5–Fig. 7. The simulation parameters are listed in Table 1. In fact, parameters L and R may largely deviate from their nominal values. In order to analyze the performance of the proposed DO-PBC with system disturbances, parameters deviation are conducted by adopting "inaccurate" nominal parameters (L_{n}=150%L and R_{n}=200%R) in controllers [35]. As shown in Fig.5, the poles of the closed-loop system (20) are all located at the left half of the *s*-plane and indicate that the control is stable. Moreover, one can see none of the pole-zeros induce overshoot in Zone I and III, practically speaking, because the damping coefficient is larger than 0.8. After most of the poles are canceling the zeros, there are three poles remained in Zone III, however, the zero in Zone II may lead to overshoot or peak effect due to the model inversion ($P_{\mathrm{n}}^{-1}(s)$) at feedforward path, as shown in step response Fig. 6. To prevent the peaking effect of feedforward path from propagating into the *d*- and *q*- current, a saturation function or rate limiter can be employed at feedforward path $Q(s)/P_{\mathrm{n}}(s)$ [37]. Fig. 6 shows the unit step response of the closed-loop transfer function G'_{qq}. As a result, irrespective of the STATCOM system parameters deviation, the proposed DO-PBC can exactly track the reference current in steady state and offer a fast dynamic response. According to (23) and Fig.7, it can be observed that the amplitude and phase of the tracking error will be 0 dB and 0° at low and medium frequency range. The influence of the coupling terms is shown in Fig. 7 (b). It can be seen that the magnitude of G'_{dq} is much less than -30 dB, especially at the low frequency range, which means that the coupling components between the *d*- and *q*-channels are virtually nonexistent.

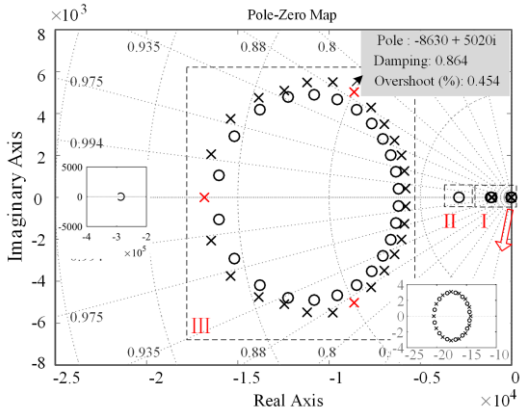

Fig. 5 Locations of the closed-loop system zeros and poles.

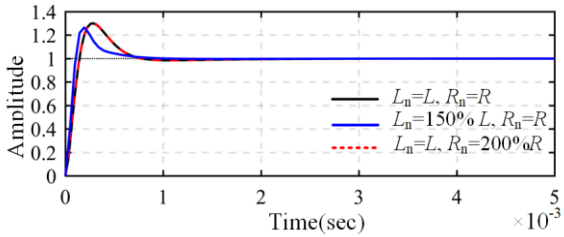

Fig. 6 Unit step response of the closed-loop transfer function $G_{qq}^{'}$ of proposed DO-PBC.

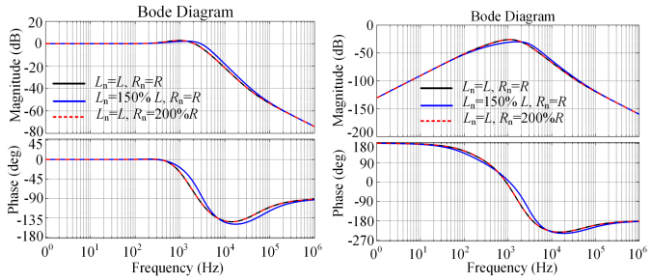

(a) (b)

Fig. 7 Closed-loop Bode diagram of proposed DO-PBC (a) $G_{qq}^{'}$, (b) $G_{dq}^{'}$.

C. Tuning of Parameters

The tuning principles of the required injection damping and time constant of $Q(s)$ design are given as follows.

The constraint of strictly passive. With proposed DO-PBC method, PBC control part is designed based on the nominal plant, while the model mismatch and parameter uncertainties are treated as disturbances. Condition $E(\boldsymbol{x})>0$ and $\dot{E}(\boldsymbol{x})<0$ depends on r_d. If the damping gain is negative, the system will fail to meet strict passive conditions:

$$R_n + r_d > 0 \tag{27}$$

The constraint of stability of cascaded control system. According to the cascaded control system, the inner loop controller should be much faster in response speed than the outer loop, which can decouple the outer loop and the inner loop. In order to guarantee that the inner loop of DO-PBC responses much faster than the outer voltage loop (more than 10 times), we have

$$\tau_{dc} \geq 10 \cdot L_n / 2(R_n + r_d) \tag{28}$$

According to (28), r_d satisfies

$$r_d \geq 5L_n/(\tau_{dc}) - R_n \tag{29}$$

The constraint of injection current THD. A too larger gain damping leads to an increase of the closed-loop bandwidth (as shown in Fig. 8(a)) and a decrease of the high frequency harmonic current ripple suppression, which will result in deterioration of system robustness against the measurement noise and the high frequency harmonic current ripple. Moreover, high gain damping may result in saturation of controller output.

The constraint of delays in the system. When the delays $T_D(s)$ in the system (which is caused by the sampling, the digital calculation, PWM, filters, etc) is considered and approximately equal to the first-order inertia term $T_D=1/(T_s s+1)$, the closed-loop transfer function of the DO-PBC can be expressed as

$$\begin{bmatrix} I_d(s) \\ I_q(s) \end{bmatrix} = \begin{bmatrix} G_{dd}^T & G_{dq}^T \\ G_{qd}^T & G_{qq}^T \end{bmatrix} \begin{bmatrix} I_d^*(s) \\ I_q^*(s) \end{bmatrix} \tag{30}$$

where

$$\begin{cases} G_{dd}^T = \dfrac{I_d(s)}{I_d^*(s)} = G_{qq}^T = \dfrac{I_q(s)}{I_q^*(s)} = \dfrac{(Q + r_d P_n) T_D P M_T}{M_T^2 + N^2} \\ G_{dq}^T = \dfrac{I_d(s)}{I_q^*(s)} = -G_{qd}^T = \dfrac{I_q(s)}{I_d^*(s)} = \dfrac{P T_D (Q + r_d P_n) N}{M_T^2 + N^2} \\ M_T = (1-Q)P_n + T_D P(Q + r_d P_n),\ N = (1-Q)P_n \omega L \mathrm{P} \end{cases} \tag{31}$$

Fig. 9 shows the location of the poles of the system (30) for different values of the damping gain r_d with considering the delays in the system. For larger values of damping r_d, the dominant poles move far from the real axis, which may lead to unexpected underdamped response with overshoot. This result indicates that the damping gain should not choose too large to avoid overshoot with considering the delays in the system. Thus, the values of damping gain (r_d) can be fine-tuned from small to large manually until the satisfactory response is achieved within the range of constraints condition.

Obviously, the time constant of $Q(s)$ exerts another important effect in DO-PBC. As shown in Fig.8 (b), a high cutoff frequency not only improves the disturbance attenuation, but also increases the sensitivity to noises. Moreover, Fig. 9 (b) shows the location of the poles of the system (30) for the different bandwidth of $Q(s)$ with considering the delays in the system. We see that the stability margin decreases while the dominant poles get close to the imaginary axis as the time constant of $Q(s)$ decreased. Thus, the time constant of $Q(s)$ in the real digital controller should not choose too small to avoid overshoot or even instability.

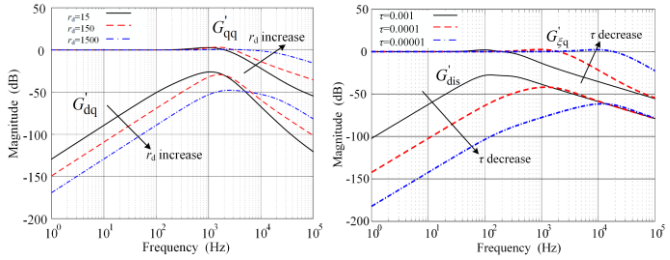

(a) (b)

Fig.8 Closed-loop Bode diagram of proposed DO-PBC (a) $G_{qq}^{'}$ and $G_{dq}^{'}$ with different damping. (b) G'_{dis} disturbance and $G'_{\xi q}$ noise suppression with different time constant τ.

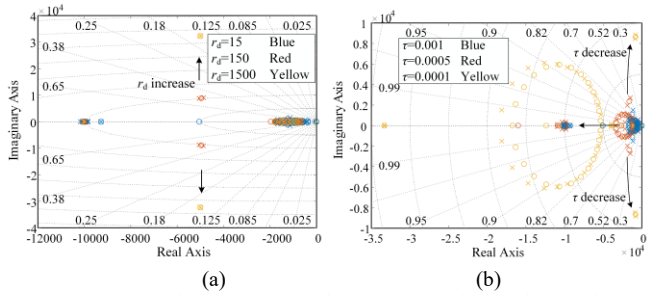

(a) (b)

Fig. 9 (a) Impact of r_d and (b) τ on the system root loci with considering the time delays.

IV. DC-LINK VOLTAGE CONTROL

For CHB STATCOM, the DC-link voltage control is essential. In this paper, the DC-link voltage control is followed by the hierarchical control structure in [6]. For considering the existing unbalanced conditions in the ac-side voltage when power system faults occur, modified DC-link voltage control is employed based on [38, 39]. Fig. 10 shows the block diagram of the DC-link voltage control. The voltage balancing control can be divided into the following: overall DC-link voltage control, cluster voltage balancing control and individual voltage balancing control.

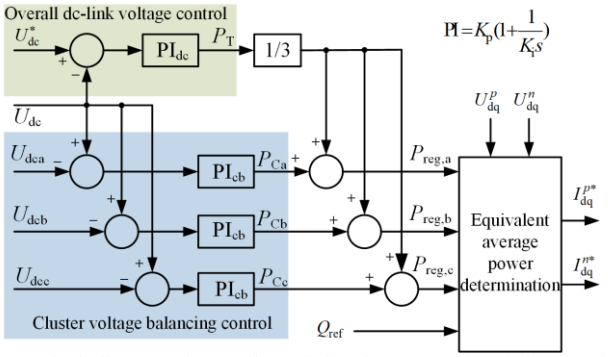

Fig. 10 Block diagram of Overall DC-link voltage control and cluster voltage control.

A. Overall DC-link voltage control and cluster voltage control considering the unbalanced AC voltage

Because of the star configuration, the point of common coupling phase voltages can be obtained by converting the line-to-line voltage into phase voltages referring to the only reference point N which contains no zero-sequence component.

$$\begin{bmatrix} u_{SA} \\ u_{SB} \\ u_{SC} \end{bmatrix} = \begin{bmatrix} u_{SA}^{p} \\ u_{SB}^{p} \\ u_{SC}^{p} \end{bmatrix} + \begin{bmatrix} u_{SA}^{n} \\ u_{SB}^{n} \\ u_{SC}^{n} \end{bmatrix} = (C_{dq}^{p})^{-1} \begin{bmatrix} U_{Sd}^{p} \\ U_{Sq}^{p} \end{bmatrix} + (C_{dq}^{n})^{-1} \begin{bmatrix} U_{Sd}^{n} \\ U_{Sq}^{n} \end{bmatrix} \quad (32)$$

where superscript p and n represent the positive and negative components. C_{dq}^{p} and C_{dq}^{n} are positive and negative Park transformation which the rotating reference frame is aligned 90 degrees behind A axis. U_{Sd}^{p}, U_{Sq}^{p}, U_{Sd}^{n} and U_{Sq}^{n} are the voltage components in positive and negative sequence rotating reference frame, respectively. Analogously, the STATCOM output current can be written as follows.

$$\begin{bmatrix} i_A \\ i_B \\ i_C \end{bmatrix} = (C_{dq}^{p})^{-1} \begin{bmatrix} I_d^{p} \\ I_q^{p} \end{bmatrix} + (C_{dq}^{n})^{-1} \begin{bmatrix} I_d^{n} \\ I_q^{n} \end{bmatrix} \quad (33)$$

The overall average active power P_T and reactive power Q_{ref} exchanged with power system can be derived as [38]

$$\begin{bmatrix} P_T \\ Q_{ref} \end{bmatrix} = \frac{3}{2} \left(\begin{bmatrix} U_{Sd}^{p} I_d^{p} + U_{Sq}^{p} I_q^{p} \\ U_{Sq}^{p} I_d^{p} - U_{Sd}^{p} I_q^{p} \end{bmatrix} + \begin{bmatrix} U_{Sd}^{n} I_d^{n} + U_{Sq}^{n} I_q^{n} \\ U_{Sq}^{n} I_d^{n} - U_{Sd}^{n} I_q^{n} \end{bmatrix} \right) \quad (34)$$

The positive- and negative- cluster average power flows ($P_{Ca}^{p}, P_{Cb}^{p}, P_{Cc}^{p}$), ($P_{Ca}^{n}, P_{Cb}^{n}, P_{Cc}^{n}$) can also derived as [38]

$$\begin{bmatrix} P_{Ca}^{p} \\ P_{Cb}^{p} \\ P_{Cc}^{p} \end{bmatrix} = \begin{bmatrix} \frac{U_{Sd}^{n}}{2} & -\frac{U_{Sq}^{n}}{2} \\ -\frac{U_{Sd}^{n}}{4} - \frac{\sqrt{3}U_{Sq}^{n}}{4} & \frac{U_{Sq}^{n}}{4} - \frac{\sqrt{3}U_{Sd}^{n}}{4} \\ -\frac{U_{Sd}^{n}}{4} + \frac{\sqrt{3}U_{Sq}^{n}}{4} & \frac{U_{Sq}^{n}}{4} + \frac{\sqrt{3}U_{Sd}^{n}}{4} \end{bmatrix} \begin{bmatrix} I_d^{p} \\ I_q^{p} \end{bmatrix} \quad (35)$$

$$\begin{bmatrix} P_{Ca}^{n} \\ P_{Cb}^{n} \\ P_{Cc}^{n} \end{bmatrix} = \begin{bmatrix} \frac{U_{Sd}^{p}}{2} & -\frac{U_{Sq}^{p}}{2} \\ -\frac{U_{Sd}^{p}}{4} - \frac{\sqrt{3}U_{Sq}^{p}}{4} & \frac{U_{Sq}^{p}}{4} - \frac{\sqrt{3}U_{Sd}^{p}}{4} \\ -\frac{U_{Sd}^{p}}{4} + \frac{\sqrt{3}U_{Sq}^{p}}{4} & \frac{U_{Sq}^{p}}{4} + \frac{\sqrt{3}U_{Sd}^{p}}{4} \end{bmatrix} \begin{bmatrix} I_d^{n} \\ I_q^{n} \end{bmatrix} \quad (36)$$

Note that the summations the positive- and negative- cluster average power flows at three phases are zero, which means that the cluster average power flows derived in (35) and (36) only exchange among STATCOM three phase legs to balance the cluster DC-link voltage. Therefore, when the unbalanced condition in the ac-side voltage happens, the required cluster average power flows for cluster voltage balancing control can be derived via (35) and (36). In addition, the overall average active power P_T is equally shared by three phase legs. Thus, the overall power regulations ($P_{reg,m}$) for the overall DC-link voltage control and cluster voltage balancing control can be derived as

$$\begin{bmatrix} P_{reg,a} \\ P_{reg,b} \\ P_{reg,c} \end{bmatrix} = \begin{bmatrix} P_{Ca}^{p} \\ P_{Cb}^{p} \\ P_{Cc}^{p} \end{bmatrix} + \begin{bmatrix} P_{Ca}^{n} \\ P_{Cb}^{n} \\ P_{Cc}^{n} \end{bmatrix} + \frac{1}{3} P_T \quad (37)$$

The required overall average active power (P_T) and cluster average power (P_{Ca}, P_{Cb}, P_{Cc}) can be obtained by PI regulators, as shown in Fig. 10. Different from the conventional method in [6], the output of PI regulators is the average power in each cluster, instead of the reference current. The outputs of PI regulators are not directly applied to the positive- and negative-sequence DO-PBC current control loop. Combining (34)-(37), one can be obtained as (38), where N_{EAP} is equivalent average power computation matrix. Since the overall power regulations ($P_{reg,m}$) are obtained by PI regulators, therefore, the reference positive- and negative-sequence currents for current inner loop can be derived as following by computing the inverse of N_{EAP} matrix.

$$\begin{bmatrix} I_d^{p*} & I_q^{p*} & I_d^{n*} & I_q^{n*} \end{bmatrix}^{T} = N_{EAP}^{-1} \begin{bmatrix} P_{reg,a} & P_{reg,b} & P_{reg,c} & Q_{ref} \end{bmatrix}^{T} \quad (39)$$

$$\begin{bmatrix} P_{\mathrm{reg,a}} \\ P_{\mathrm{reg,b}} \\ P_{\mathrm{reg,c}} \\ Q_{\mathrm{ref}} \end{bmatrix} = N_{EAP} \begin{bmatrix} I_{\mathrm{d}}^{p} \\ I_{\mathrm{q}}^{p} \\ I_{\mathrm{d}}^{n} \\ I_{\mathrm{q}}^{n} \end{bmatrix} = \begin{bmatrix} \frac{U_{\mathrm{Sd}}^{p}}{2}+\frac{U_{\mathrm{Sd}}^{n}}{2} & \frac{U_{\mathrm{Sq}}^{p}}{2}-\frac{U_{\mathrm{Sq}}^{n}}{2} & \frac{U_{\mathrm{Sd}}^{p}}{2}+\frac{U_{\mathrm{Sd}}^{n}}{2} & \frac{U_{\mathrm{Sq}}^{n}}{2}-\frac{U_{\mathrm{Sq}}^{p}}{2} \\ \frac{U_{\mathrm{Sd}}^{p}}{2}-\frac{U_{\mathrm{Sd}}^{n}}{4}-\frac{\sqrt{3}U_{\mathrm{Sq}}^{n}}{4} & \frac{U_{\mathrm{Sq}}^{p}}{2}+\frac{U_{\mathrm{Sq}}^{n}}{4}-\frac{\sqrt{3}U_{\mathrm{Sd}}^{n}}{4} & \frac{U_{\mathrm{Sd}}^{n}}{2}-\frac{U_{\mathrm{Sd}}^{p}}{4}-\frac{\sqrt{3}U_{\mathrm{Sq}}^{p}}{4} & \frac{U_{\mathrm{Sq}}^{n}}{2}+\frac{U_{\mathrm{Sq}}^{p}}{4}-\frac{\sqrt{3}U_{\mathrm{Sd}}^{p}}{4} \\ \frac{U_{\mathrm{Sd}}^{p}}{2}-\frac{U_{\mathrm{Sd}}^{n}}{4}+\frac{\sqrt{3}U_{\mathrm{Sq}}^{n}}{4} & \frac{U_{\mathrm{Sq}}^{p}}{2}+\frac{U_{\mathrm{Sq}}^{n}}{4}+\frac{\sqrt{3}U_{\mathrm{Sd}}^{n}}{4} & \frac{U_{\mathrm{Sd}}^{n}}{2}-\frac{U_{\mathrm{Sd}}^{p}}{4}+\frac{\sqrt{3}U_{\mathrm{Sq}}^{p}}{4} & \frac{U_{\mathrm{Sq}}^{n}}{2}+\frac{U_{\mathrm{Sq}}^{p}}{4}+\frac{\sqrt{3}U_{\mathrm{Sd}}^{p}}{4} \\ \frac{3U_{\mathrm{Sq}}^{p}}{2} & -\frac{3U_{\mathrm{Sd}}^{p}}{2} & \frac{3U_{\mathrm{Sq}}^{n}}{2} & -\frac{3U_{\mathrm{Sd}}^{n}}{2} \end{bmatrix} \begin{bmatrix} I_{\mathrm{d}}^{p} \\ I_{\mathrm{q}}^{p} \\ I_{\mathrm{d}}^{n} \\ I_{\mathrm{q}}^{n} \end{bmatrix} \tag{38}$$

B. Individual Voltage Balancing Control

The individual voltage balancing control is aimed to balance each of the 10 DC voltages in the same cluster equaling to the DC mean voltage of the corresponding cluster. *P* regulator is employed for individual voltage balancing control. Then, the minor compensating voltage for a-phase *i*th H-bridge cell can be expressed as

$$\Delta u_{\mathrm{dc}ai} = \begin{cases} K_{\mathrm{ib}}(U_{\mathrm{dcavg},a} - U_{\mathrm{dc}ai})\cos\omega t, & Q_{\mathrm{ref}} > 0 \\ -K_{\mathrm{ib}}(U_{\mathrm{dcavg},a} - U_{\mathrm{dc}ai})\cos\omega t, & Q_{\mathrm{ref}} < 0 \end{cases} \tag{40}$$

V. Simulation Results

In this section, a 10kV CHB STATCOM, based on the system schematic diagram shown in Fig.1, is built in MATLAB Simulink to verify the effectiveness of the proposed DO-PBC method. The system parameters are listed in Table I.

TABLE I
SIMULATION PARAMETERS

Parameter	Value
Source voltage and frequency	V_{LL}=10kV, f=50Hz
System impedance	R_{s}=0.2Ω, L_{s}=2mH
DC-link capacitor	C=6000 μF
L filter	L=14mH, R=0.24Ω
Cascade number	10
DC voltage reference	1000 V
Switching frequency	1 kHz
Injection damping	r_{d}=15
Q filter time constant	0.0001
Overall control	K_{dcp}=287, K_{dci}=0.05
Cluster balancing control	K_{cbp}=287, K_{cbi}=0.05
Individual balancing control	K_{ib}=0.3

A. Steady and Dynamic Performance of Proposed DO-PBC and Conventional PBC without Parameters uncertainties

Fig. 11 and Fig. 12 show the comparison of the steady-state and dynamic responses of the STATCOM with the proposed DO-PBC and conventional PBC schemes without parameters uncertainties. The linear load is set to 600Kw+*j*600kVar at the beginning. At *t*=0.1s, STATCOM is switched on. At *t*=0.3s, a sudden load 400kW+*j*400kVar (40%) increase is made to simulate the dynamic response. At *t*=0.4*s*, the load changes from inductive to capacitive 600kW-*j*600kVar. As shown in the Fig. 11 and Fig. 12, without parameters uncertainties, the proposed PBC and conventional PBC both can track the reference current with zero steady-state current error. However, it can be observed in Fig. 12(c) and (d) that the proposed DO-PBC strategy shows the faster response, better exact tracking performance, and robustness than the conventional PBC, especially in transient response. During the dynamic response, the transient tracking error can be regarded as disturbances. Due to the disturbance rejection performance, the transient tracking error can be effectively attenuated by DO-PBC.

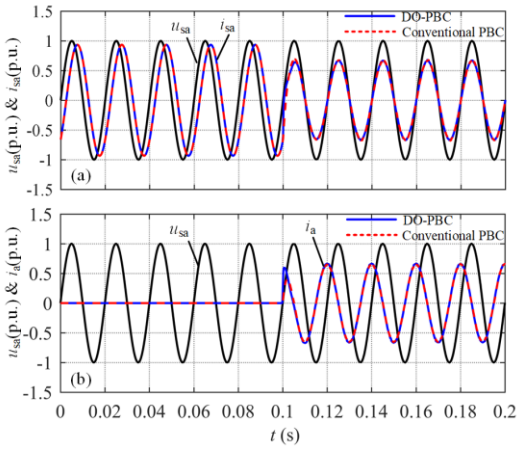

Fig. 11 Steady state response of proposed DO-PBC and conventional PBC under inductive load condition without parameters uncertainties. (a) grid voltage and current of phase-A. (b) grid voltage and STATCOM current of phase-A.

B. Control Performance Under Parameters uncertainties

To investigate the effect of the STATCOM parameters uncertainties on the control performance of the conventional PBC and the proposed DO-PBC, the simulations with three sets deviation of the real inductance *L* and the resistor *R*, i.e. (150%*L*, *R*), (*L*, 200%*R*) and (*L*, 300%*R*) have done, as shown in Fig. 13-Fig. 15. Comparing with Fig. 13 and Fig. 14, as the equivalent resister *R* deviation gets larger, the steady state error with the conventional PBC scheme will be larger. The bigger damping r_{d}, the smaller steady state tracking error. And

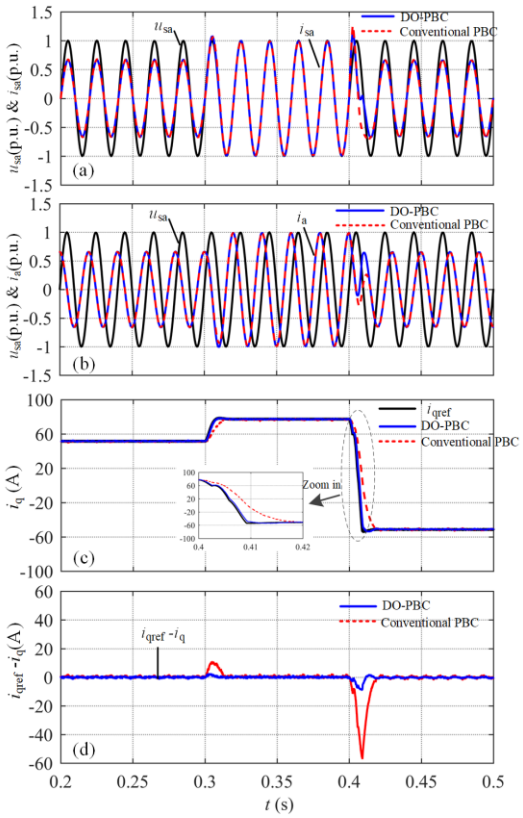

Fig. 12 Dynamic response of proposed DO-PBC and conventional PBC under load variation from inductive to capacitive without parameters uncertainties. (a) Grid voltage and current of phase-A. (b) Grid voltage and STATCOM current of phase-A. (c) q-axis current. (d) q-axis error current.

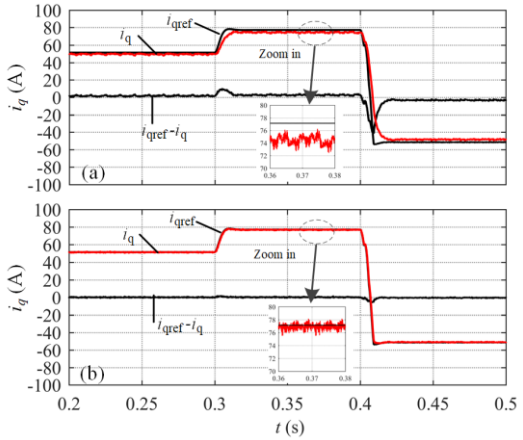

Fig. 13 Steady-state and dynamic response of the STATCOM with parameter uncertainties (L_n=L, R_n=R+100%R) under load variation. (a) Conventional PBC. (b) Proposed DO-PBC.

the proposed DO-PBC can achieve high tracking accuracy under parameters deviation. It can be observed from Fig. 15 that the parameter L deviation has a slight effect on the steady-state error of reactive power i_q^* of the conventional PBC scheme. From (12), the closed-loop transfer function at DC component is G_E=(R-R_n)/(R+r_d). However, it can be seen in Fig. 15(a) and Fig. 15(c), the conventional PBC has a relatively poor dynamic performance and incapable of

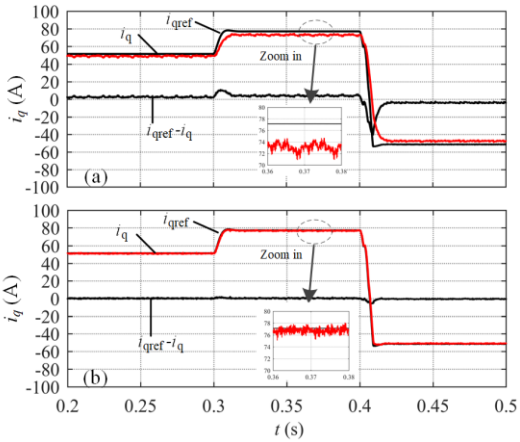

Fig. 14 Steady-state and dynamic response of the STATCOM with parameter uncertainties (L_n=L, R_n=R+200%R) under load variation. (a) Conventional PBC. (b) Proposed DO-PBC.

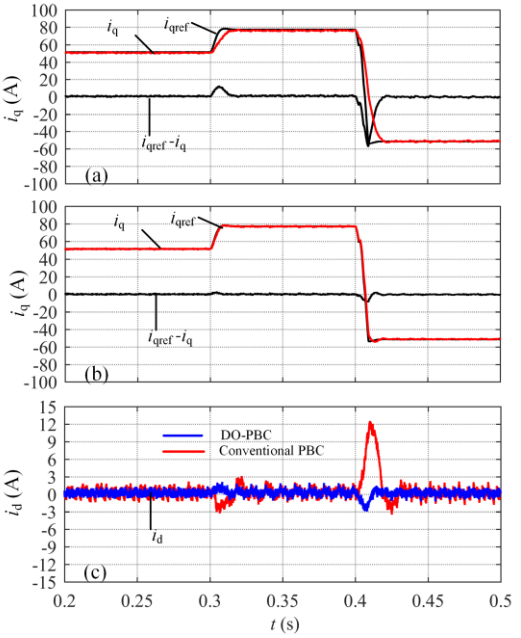

Fig. 15 Steady-state and dynamic response of the STATCOM with parameter uncertainties (L_n=150%L, R_n=R) under load variation. (a) Conventional PBC. (b) Proposed DO-PBC (c) d-axis current i_d.

eliminating the coupling terms between the d- and q- channels under parameter L deviation. Therefore, the comparison simulation results indicate that, compared with conventional PBC method, the proposed DO-PBC method can track the reference current with zero steady-state error, having a fast transient response and nonexistent coupling terms between the d- and q- channels with the presence of system uncertainties.

C. Control Performance Under Large Disturbance of Transient Faults in the Power Grid

In the real distribution system, unbalanced conditions in the ac-side voltage are unavoidable when power grid faults occur. The transient faults can be also regarded as large disturbances to check the robustness of the controller. In order to verify the performances of the proposed method under large disturbances,

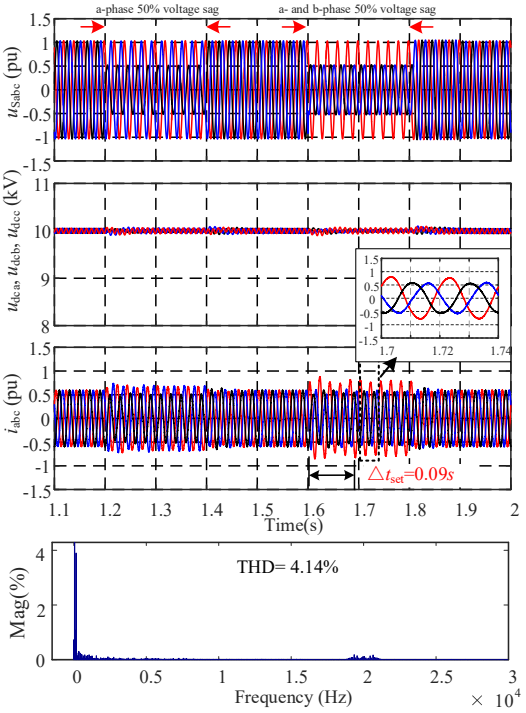

Fig. 16 Simulation waveforms with the PI method control as 50% single-phase and two-phase voltage sag.

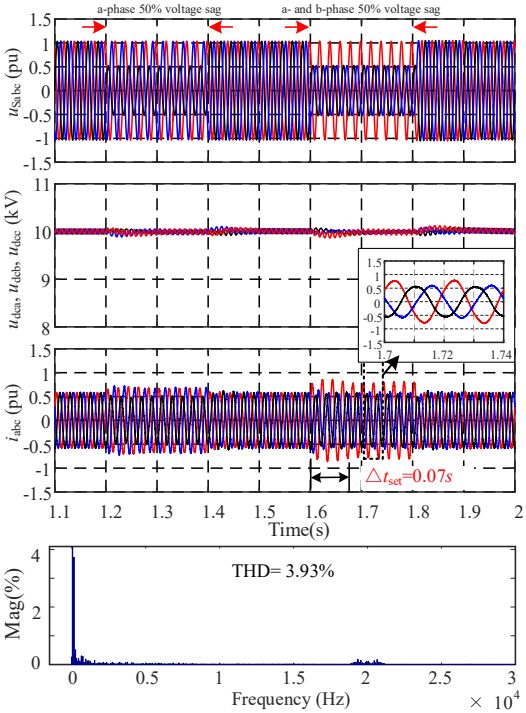

Fig. 17 Simulation waveforms with the conventional PBC as 50% single-phase and two-phase voltage sag.

faults conditions in the ac-side voltage, i.e. single-phase 50% voltage sag, two-phase 50% voltage sag, and three-phase 50% voltage sag are tested. For considering the existing unbalanced conditions in the ac-side voltage when power system faults occur, the DC-link voltage control in Section IV is employed. The power system single phase 50% voltage sag occurs at

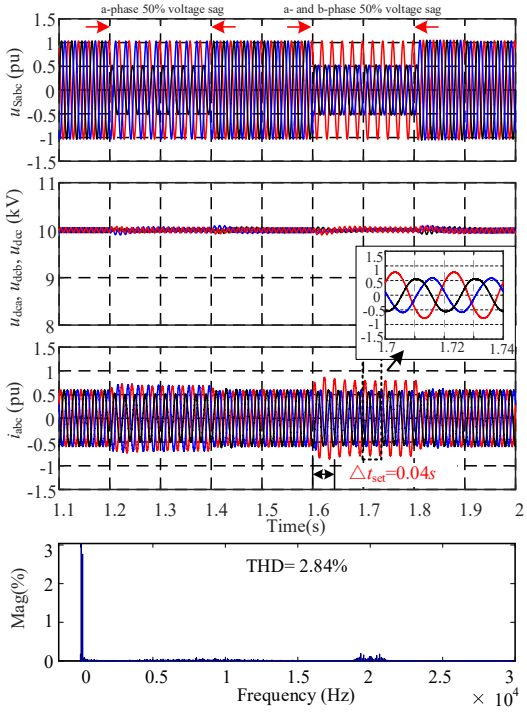

Fig. 18 Simulation waveforms with the proposed DO-PBC method control as 50% single-phase and two-phase voltage sag.

TABLE II
COMPARISONS THD PERFORMANCE AMONG PI, PBC AND DO-PBC
(Unit: %).

	Steady-state	A phase 50% voltage sags			two phase 50% voltage sags		
	i_A	i_A	i_B	i_C	i_A	i_B	i_C
PI	1.01	5.00	3.32	2.58	4.14	3.94	2.28
PBC	0.97	4.24	2.90	2.40	3.93	3.61	2.44
DO-PBC	0.54	2.63	1.43	1.50	2.84	2.75	1.37

t=1.2s, while two phase 50% voltage sag occurs at t=1.6s. Fig. 16 to Fig. 18 show the comparison results among the PI method, the conventional PBC method, and the proposed method under single-phase 50% voltage sag and two-phase 50% voltage sag. Fig. 19 shows the response of the proposed DO-PBC method under three-phase 50% voltage sag. Table II summarizes the Total Harmonic Distortion (THD) of three phases STATCOM output currents during the grid voltages unbalanced. It can be observed that both three methods can operate under unbalanced voltage conditions. However, the PI method results in longer settling time during large voltage sag disturbances. Moreover, as shown in Table II, due to excellent disturbance rejection ability of the proposed DO-PBC, the DO-PBC is with lowest THD of STATCOM output current during large voltage sag disturbances compared with PI and conventional PBC method. Therefore, the proposed DO-PBC can faster reject the external large disturbances and achieve well performances during faults in ac grid.

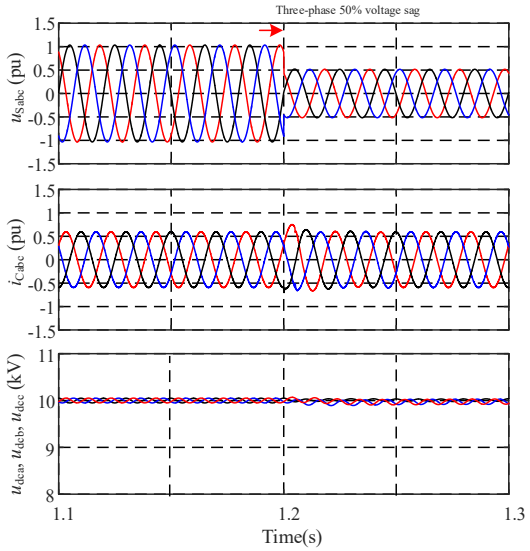

Fig. 19 Simulation waveforms with the proposed DO-PBC method control as 50% three-phase voltage sag.

VI. Experimental Results

In order to verify the STATCOM with the proposed DO-PBC method, the experiments are carried out on a down-scale 380V prototype system. As shown in Fig. 20(a) and (b), the system consists of a control box, a 7-level single-star bridge-cells STATCOM with L-filter, a 25-A active power filter (APF) and Hall sensors. The FPGA (Altera EP3C25E144I7) implements the Carrier-Phase-Shift SPWM and generates 36 PWM signals for CHB cells. Experimental hardware setup is shown in Fig. 13(b). Experiment parameters are listed in Table III. The DC-link voltage control in [6] is employed in the experiment studies without considering the unbalanced conditions in the ac-side voltage.

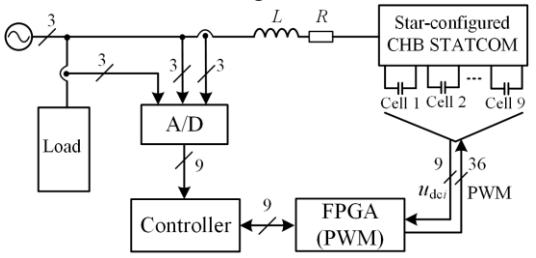

(a)

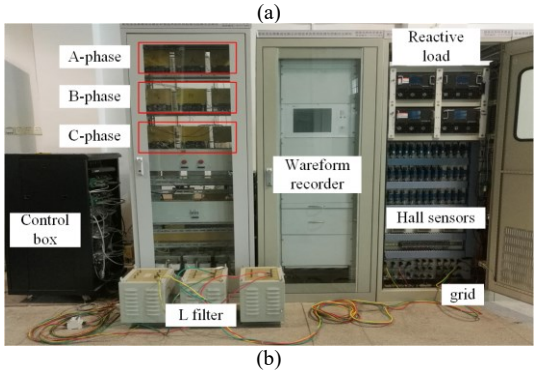

(b)

Fig. 20 Prototype 380V STATCOM. (a) Block diagram. (b) Experimental hardware setup.

TABLE I
EXPERIMENT PARAMETERS

Parameter	Value
Source voltage and frequency	V_{LL}=380 V, f=50 Hz
DC-link capacitor	C=6000 μF
DC-link voltage reference	130V
L filter	L=6 mH
Cascade number	N=3
Switching frequency	2 kHz
Injection damping	r_d=5
Q filter time constant	τ=0.00025
Overall control	K_{dcp}=0.25, K_{dci}=0.05
Cluster balancing control	K_{cb}=0.3
Individual balancing control	K_{ib}=0.1

A. Steady-State Performance

The experiment performed with a 30 Ω resistive load (4.8 kW) that acts as an active load and the APF is tuned to generate a 10A (amplitude) reactive current to simulate a 4.6 kVar reactive load (inductive).

Fig. 21 illustrates the steady-state experimental waveforms voltage and current of STATCOM with proposed DO-PBC method. The DC-link voltage and the seven-level output voltage of the STATCOM is shown in Fig. 21(a). It can be seen that the DC-link voltage is to be maintained at its reference value (130V). The resultant waveforms of the compensating current are smooth and they have small distortion under the capacitive mode and the inductive mode, as shown in Fig. 21(b) and Fig. 21(c). The grid current and voltage are in phase while STATCOM is operating.

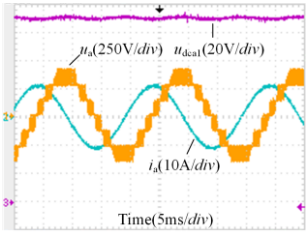

(a)

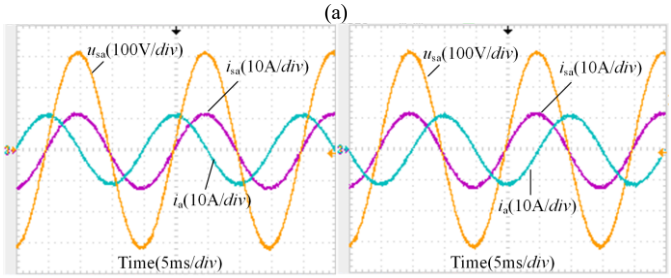

(b) (c)

Fig. 21 Experimental waveforms of the steady state phase voltage and current. (a) DC-link voltage and the seven-level output voltage of the STATCOM. (b) Inductive mode. (c) Capacitive mode.

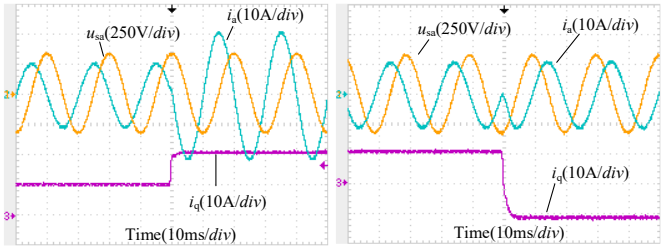

Fig. 22 Experimental waveforms of dynamic performance under a step change in the reactive power. (a) The reactive load suddenly changes from 10 A to 20 A. (b) The reactive load suddenly changes from inductive to the capacitive load.

B. Dynamic Performance under a Step Change in the Reactive Power

This experiment aims to investigate the performance of the proposed DO-PBC during a step change of load. Toward this end, the reactive load current generated by the APF is firstly set to 10A (amplitude, inductive load) and two sets of experiments are conducted: 1) the reactive load is changed suddenly from 10 A to 20 A. 2) and the reactive load is also changed in the same event from inductive (10 A) to capacitive (10 A). It can be observed from Fig. 22 that the STATCOM output current tracks the step change of reference current smooth with a fast dynamic response and a low-current overshoot. This means that the proposed DO-PBC is more effective with good transient and steady-state performance conditions.

C. Comparisons Control Performance under Parameters uncertainties

This experiment is concerned about the control performance evaluation of the proposed DO-PBC, PI and conventional PBC method under parameters uncertainties. To do so, the parameters deviation are conducted by changing the nominal parameters (L_n=150%L, R_n=0.3 Ω) in controllers design [40]. Fig. 23(a) - Fig. 23(c) shows the steady-state and dynamic response waveforms with the PI, the conventional PBC and the DO-PBC under parameters deviation L_n=L, R_n=0.3 Ω, respectively. It can be observed that a steady-state error always exists with conventional PBC method. The DO-PBC method and PI method both can achieve zero steady-state current tracking error under parameters uncertainties. Fig. 23(d) shows the error convergence after proposed DO-PBC is switching to the control system when there is a trigger signal (Fig. 23(d) CH4). Due to the model uncertainties rejection performance of DO-PBC, it can be seen that the steady-state tracking error can be removed quickly after DO-PBC working. Fig. 24 shows that the steady-state and dynamic response waveforms with the PI, the conventional PBC, and the DO-PBC under parameters deviation L_n=150%L, R_n=R, respectively. It can be observed from Fig. 24 that the parameter L deviation has a slight effect on the steady state error performance. However, the PI method has a poor dynamic performance and 10% overshoot due to the integral action, as shown in Fig.23 (a). The proposed DO-PBC can achieve a quicker dynamic response, as shown in Fig.23 (c).

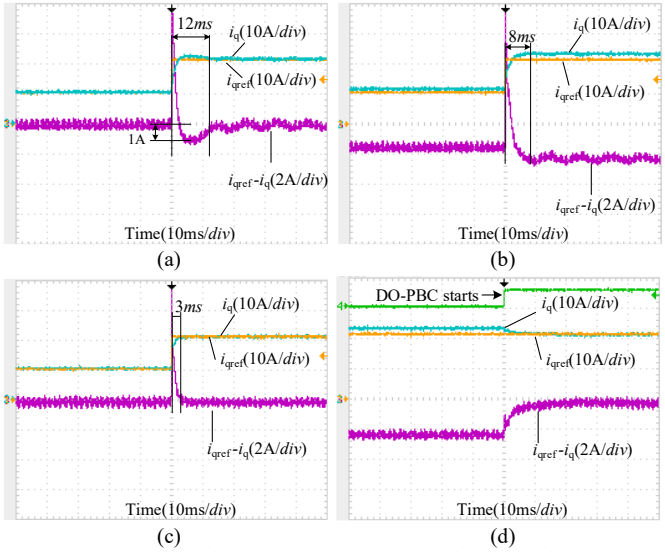

Fig. 23 Steady-state and dynamic performance evaluation under parameters uncertainties L_n=L, R_n=0.3 Ω. (a) PI method. (b) Conventional PBC . (c) Proposed DO-PBC. (d) Conventional PBC switches to the DO-PBC.

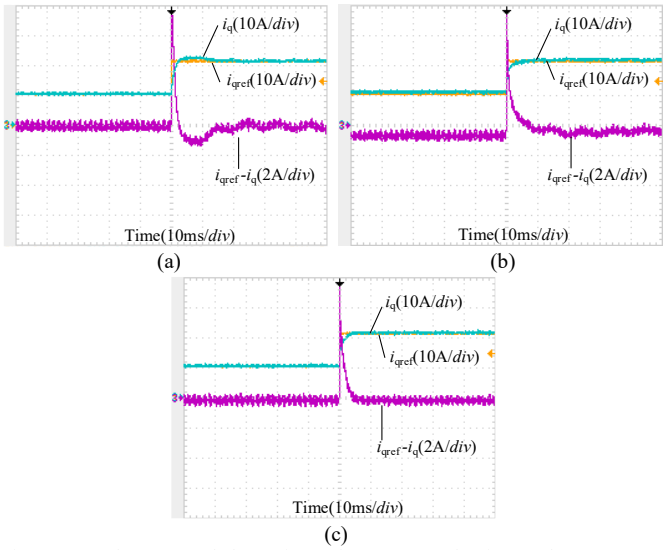

Fig. 24 Steady-state and dynamic performance evaluation under parameters uncertainties L_n=150%L, R_n=R. (a) PI method. (b) Conventional PBC . (c) Proposed DO-PBC.

D. Decoupling effectiveness Under Parameters uncertainties

This experiment is conducted to evaluate the decoupling effectiveness of the proposed DO-PBC and conventional PBC under system parameters deviation. To test the decoupling performance, the parameters deviation are conducted by changing the nominal parameters (L_n=150%L, R_n=R) in controllers design. Fig. 25 depicts the dynamic response for a reactive load current step from 10 to 20A, with the PI, the conventional PBC, and the DO-PBC method, respectively. As shown in Fig. 25 (c), it can be concluded that the proposed DO-PBC is capable for controlling of d- and q-channels independently. In contrast, from Fig. 25(a) and (b), the active current will inevitably be affected by the reactive current step change if the PI and the conventional PBC method are employed.

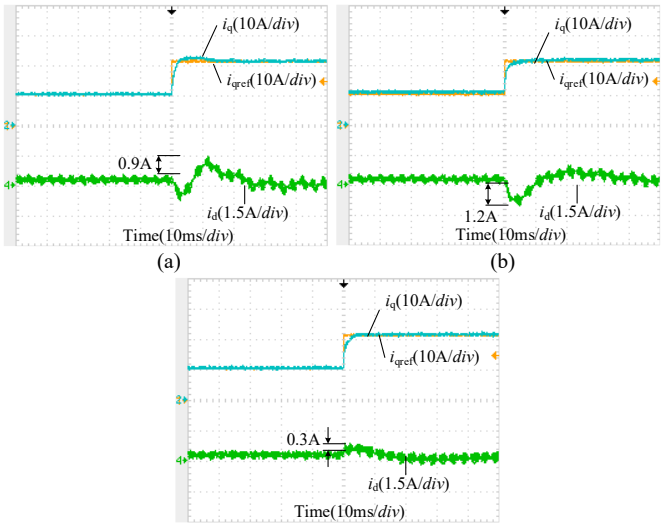

Fig. 25 Decoupling performance of proposed DO-PBC and conventional PBC under parameters uncertainties L_n=150%L, R_n=R. (a) PI method. (b) Conventional PBC . (c) Proposed DO-PBC.

All those demonstrated results are the evidence of efficient performance of the proposed DO-PBC. The proposed method fuses the merits of PBC and DO, and shows the better system disturbances rejection performance in steady-state current tracking. Moreover, the dynamic response and the decoupling performance are much better than that of PI and conventional PBC. In addition, due to the introducing of the Q-filter, the model-based inverse $1/P_n(s)$ is realizable and the robustness is significantly improved.

VII. Conclusions

This paper proposed a DO-PBC method for STATCOM to achieve system disturbances rejection and improve the robustness and the dynamic performance. The overall conclusions can be summarized as follows.

1) The theoretical analysis of the conventional PBC has shown that the conventional PBC has a poor steady-state and dynamic performance under system disturbances which include parameters uncertainties, modeling errors and external disturbances.

2) A novel DO-PBC method is proposed for STATCOM to track the current references precisely and decouple the control system effectively, thereby improving the system steady-state and dynamic control performance.

3) The detail design process, stability and robustness analysis, and parameters tuning of the proposed method are investigated, that indicates that the proper design of damping gain and DOB can ensure asymptotic stability, and has better robustness against system disturbances, such as parameters uncertainties and disturbances.

4) Compared with the PI and the conventional PBC method, the proposed DO-PBC shows the following features under system uncertainties conditions: a) The DO-PBC method could achieve zero steady-state current tracking error under parameters deviation; b) It has quicker dynamic response; c) The coupling components between the d- and q-channels can be attenuated effectively; d) Faster responses in handling not only constant disturbances but also many other types of disturbances, including the parameter uncertainties, unmodeled dynamic, and external disturbances.

5) The effectiveness of the proposed DO-PBC has been verified by simulation and experimental tests.

References

[1] B. Singh, V. Verma, and J. Solanki, "Neural Network-Based Selective Compensation of Current Quality Problems in Distribution System," *IEEE Trans. Ind. Electron.*, vol. 54, no. 1, pp. 53-60, Feb. 2007.

[2] S. Rajakaruna, A. Ghosh, and F. Shahnia, *Static Compensators (STATCOMS) in Power Systems*. New York, NY, USA: Springer, 2015.

[3] B. Gultekin and M. Ermis, "Cascaded multilevel converter-based transmission STATCOM: System design methodology and development of a 12 kV ±12 MVAr power stage," *IEEE Trans. Power Electron.*, vol. 28, no. 11, pp. 4930–4950, Nov. 2013.

[4] B. Gultekin, C. O. Gerceket, T. Atalik, et al., "Design and Implementation of a 154-kV pm 50-Mvar Transmission STATCOM Based on 21-Level Cascaded Multilevel Converter," *IEEE Trans. Ind. Appl.*, vol. 48, no. 3, pp. 1030-1045, May-June 2012.

[5] E. Lei, X. Yin, Z. Zhang and Y. Chen, "An Improved Transformer Winding Tap Injection DSTATCOM Topology for Medium-Voltage Reactive Power Compensation," *IEEE Trans. Power Electron.*, vol. 33, no. 3, pp. 2113-2126, March 2018

[6] H. Akagi, S. Inoue, and T. Yoshii, "Control and Performance of a Transformerless Cascade PWM STATCOM With Star Configuration," *IEEE Trans. Ind. Appl.*, vol. 43, no. 4, pp. 1041-1049, July-aug. 2007.

[7] L. Maharjan, S. Inoue and H. Akagi, "A Transformerless Energy Storage System Based on a Cascade Multilevel PWM Converter With Star Configuration," *IEEE Trans. Ind. Appl.*, vol. 44, no. 5, pp. 1621-1630, Sept.-Oct. 2008.

[8] C. H. Liu and Y. Y. Hsu, "Design of a Self-Tuning PI Controller for a STATCOM Using Particle Swarm Optimization," *IEEE Trans. Ind. Electron.*, vol. 57, no. 2, pp. 702-715, Feb. 2010.

[9] Y. Xu and F. Li, "Adaptive PI Control of STATCOM for Voltage Regulation," *IEEE Trans. Power Del.*, vol. 29, no. 3, pp. 1002-1011, June 2014.

[10] B. Bahrani, S. Kenzelmann and A. Rufer, "Multivariable-PI-Based dq Current Control of Voltage Source Converters With Superior Axis Decoupling Capability," *IEEE Trans. Ind. Electron.*, vol. 58, no. 7, pp. 3016-3026, July 2011.

[11] B. Bahrani, A. Karimi, B. Rey and A. Rufer, "Decoupled dq-Current Control of Grid-Tied Voltage Source Converters Using Nonparametric Models," *IEEE Trans. Ind. Electron.*, vol. 60, no. 4, pp. 1356-1366, April 2013.

[12] B. Bahrani, "*Advanced Control Strategies for Voltage Source Converters in Microgrids and traction networks*," École polytechnique fédérale de Lausanne, 2012.

[13] M. R. Nasiri, S. Farhangi and J. Rodriguez, "Model Predictive Control of Multilevel CHB STATCOM in Wind Farm Application Using Diophantine Equations," *IEEE Trans. Ind. Electron.*, vol. 66, no. 2, pp. 1213-1223, Feb. 2019.

[14] N. Kumar, T. K. Saha and J. Dey, "Sliding-Mode Control of PWM Dual Inverter-Based Grid-Connected PV System: Modeling and Performance Analysis," *IEEE J. Emerg. Sel. Top. Power Electron.*, vol. 4, no. 2, pp. 435-444, June 2016.

[15] R. Ortega, A. Loria, P. J. Nicklasson, and H. Sira-Ramirez, *Passivity Based Control of Euler-Lagrange Systems: Mechanical Electrical and Electromechanical Application*. London, U.K.: Springer-Verlag, 1998.

[16] Yang B, Jiang L, Yu T, et al, "Passive control design for multi-terminal VSC-HVDC systems via energy shaping" *Int. J. Electr. Power Energy Syst.*, 98:496-508, 2018.

[17] M. A. Hassan, T. Li, C. Duan, S. Chi, and E. P. Li, "Stabilization of DC-DC buck power converter feeding a mixed load using passivity-based control with nonlinear disturbance observer," 2017 IEEE Conference on Energy Internet and Energy System Integration (EI2), Beijing, 2017, pp. 1-6.

[18] Lopez-Garcia, Espinosa-Perez, Siguerdidjane, et al, “On the passivity-based power control of a doubly-fed induction machine,” *Int. J. Electr. Power Energy Syst.*, vol. 45, no.1, pp.303-312, 2013.

[19] M. Mehrasa, M. E. Adabi, E. Pouresmaeil, et al, “Passivity-based control technique for integration of DG resources into the power grid,” *Int. J. Electr. Power Energy Syst.*, vol. 58, no. 2, pp. 281-290, 2014.

[20] R. V. Meshram, M. Bhagwat, S. Khade, S. R. Wagh, A. M. Stanković and N. M. Singh, "Port-Controlled Phasor Hamiltonian Modeling and IDA-PBC Control of Solid-State Transformer," *IEEE Trans. Control Syst. Technol.,* vol. 27, no. 1, pp. 161-174, Jan. 2019.

[21] F. M. Serra, C. H. D. Angelo, D. G. Forchetti, “Interconnection and damping assignment control of a three-phase front end converter,” *Int. J. Electr. Power Energy Syst.*, vol. 60, no.11, pp.317-324, 2014.

[22] Tzann-Shin Lee, "Lagrangian modeling and passivity-based control of three-phase AC/DC voltage-source converters," *IEEE Trans. Ind. Electron.*, vol. 51, no. 4, pp. 892-902, Aug. 2004.

[23] Y. Lei, X. Lin and Y. Zhu, "Passivity-Based Control Strategy for SMES Under an Unbalanced Voltage Condition," IEEE Access, vol. 6, pp. 28768-28776, 2018.

[24] R. Xu et al., "A Novel Control Method for Transformerless H-Bridge Cascaded STATCOM With Star Configuration," *IEEE Trans. Power Electron.*, vol. 30, no. 3, pp. 1189-1202, March 2015.

[25] Y. Gui, W. Kim, C. C. Chung, “Passivity-Based Control With Nonlinear Damping for Type 2 STATCOM Systems,” *IEEE Trans. Power Syst.*, vol. 31, no. 4, pp. 2824-2833, 2016.

[26] X. Mu, J. Wang, W. Wu. and F. Blaabjerg, "A Modified Multifrequency Passivity-Based Control for Shunt Active Power Filter With Model-Parameter-Adaptive Capability," *IEEE Trans. Ind. Electron.*, vol. 65, no. 1, pp. 760-769, Jan. 2018.

[27] T. Qian, S. Miao, Z. Liu, et al, “Passive Control and Auxiliary Sliding Mode Control Strategy for VSC-HVDC System Based on PCHD Model,” Transactions of China Electrotechnical Society, vol.31, no. 3, pp. 138-144, 2016.

[28] M. M. Namazi, S. m. Saghaian nezhad, A. Tabesh, A. Rashidi and M. Liserre, "Passivity-based Control of Switched Reluctance-based Wind System Supplying Constant Power Load," *IEEE Trans. Ind. Electron.*, vol. 65, no. 12, pp. 9550-9560, Dec. 2018.

[29] Y. Chen, M. Wen, E. Lei, et al, “Passivity-based control of cascaded multilevel converter based D-STATCOM integrated with distribution transformer,” *Electr. Power Syst. Res.*, 154, pp. 1-12, 2018.

[30] Y. Sang, B. Yang, W. Yao, and L. Jiang, "Design and implementation of perturbation observer-based robust passivity-based control for VSC-MTDC systems considering offshore wind power integration," *IET Gener. Transm. Distrib.*, vol. 12, no. 10, pp. 2415-2424, 5 29 2018.

[31] J. Linares-Flores, J. L. Barahona-Avalos, H. Sira-Ramirez, and M. A. Contreras-Ordaz, "Robust Passivity-Based Control of a Buck–Boost-Converter/DC-Motor System: An Active Disturbance Rejection Approach," *IEEE Trans. Ind. Appl.*, vol. 48, no. 6, pp. 2362-2371, Nov.-Dec. 2012.

[32] W. He, S. Li, J. Yang, et al, “Incremental Passivity Based Control for DC-DC Boost Converters under Time-Varying Disturbances via a Generalized Proportional Integral Observer,” *J. Power Electron.*, vol.18, no,1, pp. 147-169, 2018.

[33] W. H. Chen, J. Yang, L. Guo and S. Li, "Disturbance-Observer-Based Control and Related Methods—An Overview," *IEEE Trans. Ind. Electron.*, vol. 63, no. 2, pp. 1083-1095, Feb. 2016.

[34] S. Li, J. Yang, W. Chen, et al, “*Disturbance Observer-Based Control: Methods and Applications*,” CRC Press, Inc. 2014.

[35] Y. Wu and Y. Ye, "Internal Model-Based Disturbance Observer With Application to CVCF PWM Inverter," *IEEE Trans. Ind. Electron.*, vol. 65, no. 7, pp. 5743-5753, July 2018.

[36] Youngjin Choi, Kwangjin Yang, Wan Kyun Chung, Hong Rok Kim and Il Hong Suh, "On the robustness and performance of disturbance observers for second-order systems," *IEEE Trans. Autom. Control*, vol. 48, no. 2, pp. 315-320, Feb. 2003.

[37] J. Back , H. Shim, “Adding robustness to nominal output-feedback controllers for uncertain nonlinear systems: A nonlinear version of disturbance observer,” *Automatica*, vol. 44, no. 10, pp. 2528-2537, 2008.

[38] H. Chen, P. Wu, C. Lee, C. Wang, C. Yang, and P. Cheng, "A Flexible DC Voltage Balancing Control Based on the Power Flow Management for Star-Connected Cascaded H-Bridge Converter," *IEEE Trans. Ind. Appl.*, vol. 52, no. 6, pp. 4946-4954, Nov.-Dec. 2016.

[39] H. Chen, P. Wu, C. Lee, C. Wang, C. Yang, and P. Cheng, "Zero-Sequence Voltage Injection for DC Capacitor Voltage Balancing Control of the Star-Connected Cascaded H-Bridge PWM Converter Under Unbalanced Grid," *IEEE Trans. Ind. Appl.*, vol. 51, no. 6, pp. 4584-4594, Nov.-Dec. 2015.

[40] Y. Qi, L. Peng, M. Chen, and Z. Huang, “Load disturbance suppression for voltage-controlled three-phase voltage source inverter with transformer,” *IET Power Electron.*, vol. 7, no. 12, pp. 3147-3158, Dec. 2014